JOURNAL OF COMPUTATIONAL PHYSICS **138,** 193–223 (1997)
ARTICLE NO. CP975817

A Level Set Approach to a Unified Model for Etching, Deposition, and Lithography

III: Redeposition, Reemission, Surface Diffusion, and Complex Simulations

D. Adalsteinsson and J. A. Sethian[1]

Department of Mathematics, University of California, Berkeley and Mathematics Department,
National Lawrence Berkeley Laboratory
E-mail: dabbi@math.lbl.gov and sethian@math.berkeley.edu

Received December 23, 1996; revised August 5, 1997

Previously, Adalsteinsson and Sethian have applied the level set formulation to the problem of surface advancement in two and three-dimensional topography simulation of deposition, etching, and lithography processes in integrated circuit fabrication. The level set formulation is based on solving a Hamilton–Jacobi type equation for a propagating level set function, using techniques borrowed from hyperbolic conservation laws. Topological changes, corner, and cusp development, and accurate determination of geometric properties such as curvature and normal direction are naturally obtained in this setting. Part I presented the basic equations and algorithms for two dimensional simulations, including the effects of isotropic and uni-directional deposition and etching, visibility, reflection, and material dependent etch/deposition rates. Part II focused on the extension to three dimensions. This paper completes the series, and add the effects of redeposition, reemission, and surface diffusion. This requires the solution of the transport equations for arbitrary geometries, and leads to simulations that contain multiple simultaneous competing effects of visibility, directional and source flux functions, complex sputter yield flux functions, wide ranges of sticking coefficients for the reemission and redeposition functions, multilayered fronts and thin film layers.

---

[1] Supported in part by the Applied Mathematics Subprogram of the Office of Energy Research under Contract DE-AC03-76SF00098, and the National Science Foundation and DARPA under Grant DMS-8919074.

0021-9991/97 $25.00

1. INTRODUCTION

In this paper, we complete the development of a level set formulation to simulate deposition, etching, and lithography in integrated circuit fabrication. The goal is an accurate, stable, and efficient technique for surface advancement due to complex motion which, under different physical effects, may include effects of anisotropy, visibility conditions, material-dependent propagation rates, complex sputter laws, redeposition, reemission, and surface diffusion. In Part I of this paper, "A Level Set Approach to a Unified Model for Etching, Deposition, and Photolithography I: Two-Dimensional Simulations" [4], the basic equations and algorithms for two-dimensional simulations are developed. In Part II [5], the extension to three dimensions was presented and a large collection of simulations, including three-dimensional etching and deposition into cavities under the effects of visibility, directional and source flux functions, evolution of lithographic profiles, discontinuous etch rates through multiple materials, and nonconvex sputter yield flux functions were shown. In [42, 43] the fast marching method was introduced for solving the Eikonal equation which arises in photolithography development simulations. A review of these earlier works, aimed at the micro-electronics community, was presented in [45]. In this paper, we extend these works to fully three-dimensional topographic simulations, including the effects of redeposition, reemission, thin films, and surface diffusion. This requires the solution of transport equations for arbitrary surfaces. The validity of various physical models for microfabrication will not be examined. Instead, we hope to provide a robust numerical approach to these phenomena which can then be used to systematically examine various models.

As discussed in [4, 5], a variety of numerical algorithms are available to advance fronts in etching, deposition and photolithography processes. These methods are not unique to such simulations, and in fact are in use in such areas as dendritic growth and solidification, flame/combustion models, and fluid interfaces. They include string methods, cell fraction methods, and characteristic methods. While powerful, these methods have some weaknesses, including difficulties in executing topological change, instabilities near sharp corners and cusps, complexities in three dimensions, and lack of robustness issues. Details of these methods are given in [4, 5, 44].

Level set methods, developed by Osher and Sethian in [31], based on the theory and numerics of weak solutions to surface propagation formulated by Sethian [37, 38], offer highly robust and accurate techniques for tracking interfaces moving under complex motions. They work in any number of space dimensions, handle topological merging and breaking naturally, and are easy to program. They approximate the equations of motion for the underlying propagating surface, which resemble Hamilton-Jacobi equations with parabolic right-hand sides. The central mathematical idea is to view the moving front as a particular level set of a higher dimensional function. In this setting, sharp gradients and cusps form naturally, and the effects of curvature may be easily incorporated. The key numerical idea is to borrow the technology from the numerical solution of hyperbolic conservation laws and transfer these schemes to the Hamilton–Jacobi setting, which then guarantees that the correct entropy satisfying solution will be obtained. A comprehensive introduction and review of the state-of-the-art of level set methods may be found in [44].

2. LEVEL SET METHODS

2.1. *The General Level Set Method*

Here, we briefly summarize the key ideas behind level set methods; for details, see [31, 40, 44]. Given a moving closed hypersurface $\Gamma(t)$, we wish to produce an Eulerian formulation for the motion of the hypersurface propagating along its normal direction with speed F, where F can be a function of various arguments, including the curvature, normal direction, etc. The main idea is to embed this propagating interface as the zero level set of a higher dimensional function ϕ. Let $\phi(x, t = 0)$, where $x \in R^N$ is defined by

$$\phi(x, t = 0) = \pm d, \tag{1}$$

where d is the distance from x to $\Gamma(t = 0)$, and the plus (minus) sign is chosen if the point x is outside (inside) the initial hypersurface $\Gamma(t = 0)$. (Any smooth function will do.) Thus, we have an initial function $\phi(x, t = 0) : R^N \rightarrow R$ with the property that

$$\Gamma(t = 0) = (x|\phi(x, t = 0) = 0). \tag{2}$$

Our goal is to now produce an equation for the evolving function $\phi(x, t)$ which contains the embedded motion of $\Gamma(t)$ as the level set $\phi = 0$. Let $x(t)$, $t \in [0, \infty)$ be the path of a point on the propagating front. That is, $x(t = 0)$ is a point on the initial front $\Gamma(t = 0)$, and $x_t \cdot n = F(x(t))$, where the vector n is normal to the front at $x(t)$. Since the evolving function ϕ is always zero on the propagating hypersurface, we must have

$$\phi(x(t), t) = 0. \tag{3}$$

By the chain rule,

$$\phi_t + \nabla\phi(x(t, t)) \cdot x_t = 0. \tag{4}$$

Since F already gives the speed in the outward normal direction, then $x'(t) \cdot n = F$ where $n = \nabla\phi/|\nabla\phi|$. Thus, we then have the evolution equation for ϕ, namely

$$\phi_t + F|\nabla\phi| = 0 \tag{5}$$

$$\phi(x, t = 0) \quad \text{given.} \tag{6}$$

We refer to this as a Hamilton–Jacobi “type” equation because, for certain forms of the speed function F, we obtain the standard Hamilton–Jacobi equation.

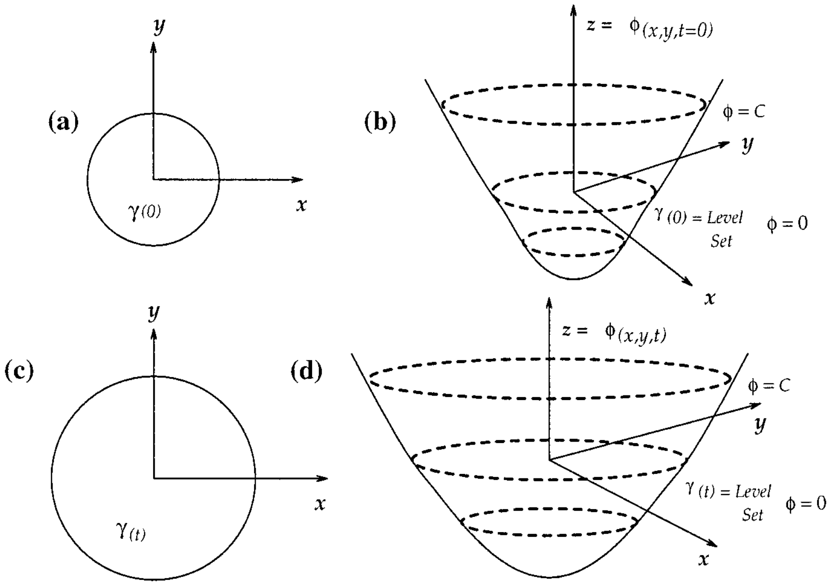

FIG. 1. Propagating circle.

In Fig. 1 (taken from [39]), we show the outward propagation of an initial curve and the accompanying motion of the level set function ϕ. In Fig. 1a we show the initial circle, and in Fig. 1c we show the circle at a later time. In Fig. 1b we show the initial position of the level set function ϕ, and in Fig. 1d we show this function at a later time.

The advantages of this approach are well known. First, the evolving function $\phi(x, t)$ always remains a function as long as F is continuous. However, the level surface $\phi = 0$, and hence, the propagating hypersurface $\Gamma(t)$ may change topology, break, merge, and form sharp corners as the function ϕ evolves; see [31]. Second, because $\phi(x, t)$ remains a function as it evolves, we may use a discrete grid in the domain of x and substitute conservative upwind finite difference approximations for the spatial and temporal derivatives. Third, intrinsic geometric properties of the front, including curvature and normal direction may be easily determined from the level function ϕ. Fourth, there are no significant differences in following fronts in three space dimensions. For details, see [44].

Since its introduction in [31], the above level set approach has been used in a wide collection of problems involving moving interfaces. Some of these applications include the generation of minimal surfaces [13], singularities and geodesics in moving curves and surfaces in [14], flame propagation [34, 50], fluid interfaces [11, 30], shape-from-shading problems [24], shape reconstruction [27], image processing [25, 26], and fast methods in [2]. The fundamental Eulerian perspective presented by this approach has since been adopted in many theoretical analyses of mean curvature flow; see in particular [17, 12], and related work in [6, 16, 18–20, 22].

2.2. *Fast Narrow Band Methods*

Rather than employ the full level set approach, we use a narrow band version which focuses computational labor on cells that bracket the zero level set corresponding to the front. This approach was introduced in [13], used in recovering images in [27], and analyzed extensively in [2]. There are two reasons to do so. The first is speed; in three dimensions, the update count for the full level set method is $O(N^3)$, where N is the number of cells in each direction. By limiting calculations to a narrow band of width k around the zero level set, the operation count drops to $O(kN^2)$, which is a substantial savings. Typically we use bandwidths of six cells in each direction, and the corresponding speedup is an order of magnitude over the full level set approach.

The second reason to employ the narrow band construction is because certain properties of the front which contribute to determining its motion have no natural meaning on other level sets. Such variables, known as extension variables, have previously been treated by the following approach; for any given level set, the value of the extension variable is found by using the value on the closest point of the zero level set. For details, see [2, 4]. In this paper, we introduce a new general technique for creating extension velocities.

Local variables, such as normal vectors and curvature have meaning for all the level sets and may be easily calculated using those values. Normals are calculated using the average one-sided difference technique discussed in [46]. Variations in etch rate, either through masks, material dependence, or lithographic etch rates are directly incorporated into the speed function.

The front is updated using second order in space schemes especially designed for the level set function; see [4, 5, 44]. There are two separate schemes; first, an ENO-based scheme for convex speed functions F which most naturally occur in lithography simulations and some source deposition problems, and a nonconvex Lax–Friedrichs/ENO scheme (see [32]), which can be required for sputter etch/deposition problems. Complete details of these schemes may be found in [4, 5, 44].

3. EQUATIONS OF MOTION FOR ETCHING AND DEPOSITION

The goal is now to build the speed function F for etching and deposition in the level set framework, namely

$$\phi_t + F|\nabla\phi| = 0 \tag{7}$$

$$\phi(x, t = 0) \quad \text{given.} \tag{8}$$

Note that F is the speed in the normal direction. Our approach is to write the normal speed function as the superposition of the two main physical effects:

$$F = F_{\text{Etching}} + F_{\text{Deposition}}. \tag{9}$$

The underlying physical effects involved in etching and deposition are quite complex; much of the following summary is obtained from the excellent overviews in [8–10, 28, 33, 35, 36, 47–49]. The two effects may be summarized briefly as follows:

- *Deposition.* Particles are deposited on the surface, which causes buildup in the profile. The particles may either isotropically condense from the surroundings (known as chemical or ‘‘wet’’ deposition), or be deposited from a source. In the latter case, we envision particles leaving the source and depositing on the surface; the main advantage of this approach is increased control over the directionality of surface deposition. The rate of deposition, and hence growth of the layer, may depend on source masking, visibility effects between the source and surface point, angle-dependent flux distribution of source particles, and the angle of incidence of the particles relative to the surface normal direction. In addition, particles may not stick, but in fact be reemitted back into the domain. This is known as ‘‘reemission’’; the ‘‘sticking coefficient’’ between zero and one is the fraction of particles that stick. Here, a sticking coefficient of unity means that all particles stick; a low sticking coefficient means that particles may bounce many times before they eventually become fixed to the surface.
- *Etching.* Particles remove material from the evolving profile boundary. The material may be isotropically removed, known again as chemical or ‘‘wet’’ etching, or chipped away through reactive ion etching, also known as ‘‘ion milling’’. Similar to deposition, the main advantage of reactive ion etching is enhanced directionality, which becomes increasingly important as device sizes decrease substantially and etching must proceed in vertical directions without affecting adjacent features. The total etch rate consists of an ion-assisted rate and a purely chemical etch rate due to etching by neutral radicals, which may still have a directional component. As in the above, the total etch rate due to wet and directional milling effects can depend on source masking, visibility effects between the source and surface point, angle-dependent flux distribution of source particles, and the angle of incidence of the particles relative to the surface normal direction. In addition, due to chemical reactions that take place on the surface, etching can cause surface particles to be ejected; this process is known as ‘‘redeposition’’; the newly ejected particles are then deposited elsewhere on the front, depending on their angle and distribution.

In the rest of this section, we formalize the above.

3.1. *Initial Position and Setup*

Define the coordinate system with the x and y axes lying in the plane and z being the vertical axis. We consider an initial profile $h(x, y)$, where h gives the height of the initial surface above the xy plane. We also consider a source Z given as a surface above the initial profile, and write $Z(x, y)$ referring to the height of the source at the point (x, y).

For both etching and deposition, define the source ray to be the ray leading the source and aimed towards the surface profile. Let ψ be the angle variation in the

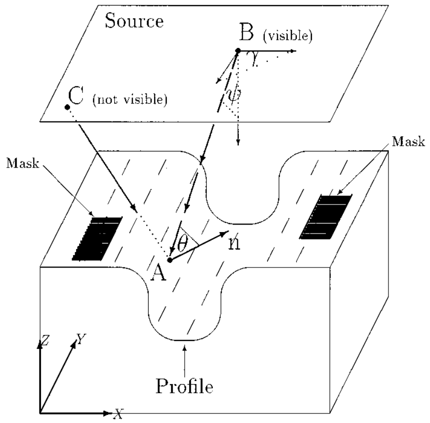

FIG. 2. Variables and setup.

source ray away from the negative z axis; ψ runs from 0 to π. Let γ be the angle between the projection of the source ray in the xy plane and the positive x axis. Let n be the normal vector at a point x on the surface profile, and θ the angle between the normal and the source ray.

In Fig. 2, we indicate these variables. Masks, which force flux rates to be zero, are indicated by heavy dark patches on the initial profile. At each point of the profile, we also assign a visibility indicator function $\Upsilon(x, x')$ which indicates whether the point x on the initial profile can be seen by the source point x'.

Our goal is to write the effects of deposition, etching, and lithography on the speed F at a point $\boldsymbol{x}$ on the front.

3.2. *Individual Terms*

3.2.1. *Etching.* We consider two separate types of etching:

- $F^{\text{Etching}}_{\text{Isotropic}}$: *Isotropic etching.* Uniform etching, also known as chemical or wet etching.
- $F^{\text{Etching}}_{\text{Direct}}$: *Direct etching.* Etching from an external source; this can be either a collection of point sources, or from an external stream coming from a particular direction. Visibility effects are included; and the flux strength can depend on both the solid angle from the emitting source and the angle between the profile normal and the incoming source direction. Etching can include highly sensitive dependence on angle such as in ion-milling.

3.2.2. *Deposition.* We consider four separate types of deposition:

- $F^{\text{Deposition}}_{\text{Isotropic}}$: *Isotropic deposition.* Uniform deposition, also known as chemical or wet deposition.

- $F^{\text{Deposition}}_{\text{Direct}}$: *Direct deposition.* Deposition from an external source; this can be either a collection of point sources, or from an external stream coming from a particular direction. Visibility effects are included; and the flux strength can depend on both the solid angle from the emitting source and the angle between the profile normal and the incoming source.

- $F^{\text{Deposition}}_{\text{Redeposition}}$: *Redeposition.* Particles that are expelled during the etching process. These particles then attach themselves to the profile at other locations; the strength and distribution of the redeposition flux function can depend on such factors as the local angle. A redeposition coefficient, $\beta_{\text{redeposition}}$ can range from zero to unity to reflect the fraction of redeposition that results from the etching process. A value of $\beta_{\text{redeposition}} = 1$ means that nothing is redeposited elsewhere; in other words, everything sticks.

- $F^{\text{Deposition}}_{\text{Reemission}}$: *Reemission deposition.* Particles that are deposited from direct deposition may in fact not stick and are then reemitted into the domain. The amount of particles reemitted depends on a sticking coefficient $\beta_{\text{reemission}}$. If $\beta_{\text{reemission}} = 1$, then this means that nothing is reemitted.

In Fig. 2, we generalize all of these effects as the "source." Thus, the plane source as shown in the figure may consist of locations which emit either unidirectional deposition or point source deposition.

3.3. *Assembling the Terms*

We may, somewhat abstractly, assemble the above terms into the single expression

$$F = F^{\text{Etching}}_{\text{Isotropic}} + F^{\text{Etching}}_{\text{Direct}} + F^{\text{Deposition}}_{\text{Isotropic}} + F^{\text{Deposition}}_{\text{Direct}} + F^{\text{Deposition}}_{\text{Redeposition}} + F^{\text{Deposition}}_{\text{Reemission}} \tag{10}$$

The two isotropic terms are evaluated at a point x by simply evaluating the strengths at that point. The two direct terms are evaluated at a point x on the profile by first computing the visibility to each point of the source and then evaluating the flux function; thus these terms require computing an integral over the entire source. To compute the fifth term at a point x, we must consider the contributions of every point on the profile to check for redeposition particles arising from the etching process; thus this term requires computing an integral over the profile itself. The sixth term, $F_{\text{Reemission}}$ is more problematic; since every point on the front can act as a deposition source of reemitted particles that do not stick, the total flux function deposition function comes from evaluating an *integral equation* along the entire profile.

In more detail, let Ω be the set of points on the evolving profile at time t, and let *Source* be the external source. Given two points x and x', let $\Upsilon(x, x')$ be one if the points are visible from one another and zero otherwise. Let r be the distance from x to x', $\boldsymbol{n}$ be the unit normal vector at the point x, and finally, let $\boldsymbol{\alpha}$ be the unit vector at the point x' on the source pointing towards the point x on the profile. Then we may refine the above terms as

$$F = \left[\begin{array}{c} \mathrm{Flux}_{\mathrm{Isotropic}}^{\mathrm{Etching}} \\ + \\ \int_{\mathrm{Source}} \mathrm{Flux}_{\mathrm{Direct}}^{\mathrm{Etching}}(r, \psi, \gamma, \theta, x)\Upsilon(x, x')(\boldsymbol{n} \cdot \boldsymbol{\alpha})\, dx' \\ + \\ \mathrm{Flux}_{\mathrm{Isotropic}}^{\mathrm{Deposition}} \\ + \\ \int_{\mathrm{Source}} \mathrm{Flux}_{\mathrm{Direct}}^{\mathrm{Deposition}}(r, \psi, \gamma, \theta, x)\Upsilon(x, x')(\boldsymbol{n} \cdot \boldsymbol{\alpha})\, dx' \\ + \\ \int_{\Omega} (1 - \beta_{\mathrm{redeposition}})\mathrm{Flux}_{\mathrm{Redeposition}}^{\mathrm{Deposition}}(r, \psi, \gamma, \theta, x)\Upsilon(x, x')(\boldsymbol{n} \cdot \boldsymbol{\alpha})\, dx' \\ + \\ \int_{\Omega} (1 - \beta_{\mathrm{reemission}})\mathrm{Flux}_{\mathrm{Reemission}}^{\mathrm{Deposition}}(r, \psi, \gamma, \theta, x)\Upsilon(x, x')(\boldsymbol{n} \cdot \boldsymbol{\alpha})\, dx' \end{array}\right]. \quad (11)$$

The integrals are performed in a straightforward manner. The front is located by constructing the zero level set of ϕ; in two dimensions it is represented by a collection of line segments; in three-dimensions by a collection of voxel elements; see [4, 5]. The centroid of each element is taken as the control point, and the individual flux terms are evaluated at each control point. In the case of the two isotropic terms, the flux is immediately found. In the case of the two integrals over sources, the source is suitably discretized and the contributions summed. In the fifth term, corresponding to redeposition, the integral over the entire profile is calculated by computing the visibility to all other control points and the corresponding redeposition term is produced by the effect of direct deposition. Thus, as presented, the fifth term requires N^2 evaluations, where N is the number of control points which approximate the front.

3.4. *Evaluation of the Reemission Term*

The sixth and last term is somewhat more time-consuming to evaluate, since the integral requires evaluation of the flux contribution $Flux_{\mathrm{Direct/Redeposition}}$ from each point of the interface, each of which depends on the contribution from all other points. Thus, this is an integral equation which must be solved to produce the total deposition flux at any point. In the below discussion, we shall assume that the total deposition flux depends on deposition directly from the source, as well as additional deposition due to particles which do not stick and are in fact reemitted.[2] We shall call this flux $Flux_{\mathrm{Direct/Redeposition}}$, and solve for it.

We now introduce some additional notation; in this discussion, we derive the appropriate integral equation for two-dimensional problems; the derivation in three dimensions is similar. Let

---

[2] Ion-induced redeposition particles can be included as part of the reemission process as well.

- t_i be the coordinates of point number i, with an associated segment length l_i,
- r_{ij} be the distance between point i and j,
- θ_j^i be the angle between the normal to point i and the vector $t_j - t_i$,
- Υ_{ij} be the visibility factor which is one if the point at x_i and x_j can see each other and zero otherwise,
- β_0 be the sticking coefficient for the particles coming directly from the source; $\beta_0 = 1.0$ means that all the particles stick,
- β be the sticking coefficient for secondary bounces,
- I_S^i be the incoming source strength at point i due to the above light source,
- I_R^i be the source strength at radiated from point i, and
- I_S and I_R be the vectors $(I_S^0, \ldots, I_S^n)$ and $(I_R^0, \ldots, I_R^n)$.

The expression for the flux is an integral equation for the received flux. Once the problem is discretized into a matrix relation, there are two numerical approaches to solving the equation. The first is to use a direct solver for the matrix equation. In two dimensions, this is practical, for large three-dimensional problems this becomes impractical due to the computational labor. The second approach is to construct an iterative solution to the integral equation, based on a series expansion of the interaction matrix. We discuss both approaches below.

3.4.1. *Direct solution of integral equation.* Our strategy is to first work with the amount I_R radiated from each point of the surface; this depends on the amount received from the direct source plus the amount radiated from all other points on the surface, that is,

$$I_R^i = (1 - \beta_0) I_S^i + (1 - \beta) \sum_{j, j \neq i} I_R^j \frac{\cos(\theta_i^j) \cos(\theta_j^i)}{2 r_{ij}} \Upsilon_{ij} l_j. \tag{12}$$

In this equation, there are several things to point out. First, we are standing at each point i and computing the contributions from the source, as well as from all other points on the front. Second, there are two contributing cosines in the expression. One is from the receiving point, which contains a cosine due the collected flux along the segment. The second cosine is due to the assumption of luminescent reflection; we assume that once a particle hits, it has an equal probability of heading off in any direction. Using the model of an assumed cosine distribution around the normal, this then generates the other cosine term.

Define the matrix Ω by

$$\Omega_{ij} = \frac{\cos(\theta_j^i) \cos(\theta_i^j)}{2 r_{ij}} \Upsilon_{ij} l_j, \tag{13}$$

when $i \neq j$, and 0 if $i = j$.

Note that since $\cos(\theta_j^i) = n_i \cdot (t_j - t_i)/|t_j - t_i|$, Ω can be rewritten as

$$\Omega_{ij} = \frac{[n_i \cdot (t_j - t_i)][n_j \cdot (t_i - t_j)]}{\pi |t_j - t_i|^3} \Upsilon_{ij} l_j. \tag{14}$$

Thus,

$$I_{\mathrm{R}} = (1 - \beta_0) I_{\mathrm{S}} + (1 - \beta)\Omega I_{\mathrm{R}}, \tag{15}$$

and we may express I_{R} in terms of I_{S} by

$$I_{\mathrm{R}} = (1 - \beta_0)(I - (1 - \beta)\Omega)^{-1} I_{\mathrm{S}}. \tag{16}$$

Thus, the received flux at the front at a point i is given by

$$Flux^i_{\mathrm{DirectDeposition/Redeposition}} = \beta_0 I^i_{\mathrm{S}} + \beta \sum_{j, j \neq i} I^j_{\mathrm{R}} \frac{\cos(\theta^j_i)\cos(\theta^i_j)}{2 r_{ij}} \Upsilon_{ij} l_j, \tag{17}$$

and, in vector form, we may rewrite this expression as

$$Flux_{\mathrm{DirectDeposition/Redeposition}} = \beta_0 I_{\mathrm{S}} + \beta \Omega I_{\mathrm{R}}. \tag{18}$$

Our goal now is to eliminate the expression I_{R} in the above. We first rearrange Eq. (15) to get

$$\Omega I_{\mathrm{R}} = \frac{1}{(1 - \beta)} I_{\mathrm{R}} - \frac{(1 - \beta_0)}{(1 - \beta)} I_{\mathrm{S}}. \tag{19}$$

Substitution into the flux equation (Eq. (18) then gives

$$Flux_{\mathrm{DirectDeposition/Redeposition}} = \frac{(\beta_0 - \beta)}{(1 - \beta)} I_{\mathrm{S}} + \frac{\beta}{(1 - \beta)} I_{\mathrm{R}}. \tag{20}$$

Finally, we may substitute the expression for I_{R} in terms of I_{S} to get

$$\frac{(\beta_0 - \beta)}{(1 - \beta)} I_{\mathrm{S}} + \frac{\beta(1 - \beta_0)}{(1 - \beta)} (I - (1 - \beta)\Omega)^{-1} I_{\mathrm{S}}. \tag{21}$$

We point out that an important special case is given when $\beta_0 = \beta$ (that is, the sticking coefficient is the same for all bounces), in which case the equation becomes

$$Flux_{\mathrm{DirectDeposition/Redeposition}} = \beta (I - (1 - \beta)\Omega)^{-1} I_{\mathrm{S}}. \tag{22}$$

We note that in these equations, Ω is nonsymmetric, thus defining

$$\Psi_{ij} = \frac{n_i \cdot (t_j - t_i) n_j \cdot (t_i - t_j)}{2 |t_j - t_i|^3} \Upsilon_{ij}, \tag{23}$$

and letting L be the diagonal matrix with $L_{ii} = l_i$, $\Omega = \Psi L$, and Ψ is symmetric. The equation therefore becomes

$$\frac{(\beta - \beta_0)}{(1 - \beta)} I_{\mathrm{S}} + \frac{\beta(1 - \beta_0)}{(1 - \beta)} (I - (1 - \beta)\Psi L)^{-1} I_{\mathrm{S}}, \tag{24}$$

$$\frac{(\beta - \beta_0)}{(1 - \beta)} I_{\mathrm{S}} + \frac{\beta(1 - \beta_0)}{(1 - \beta)} L^{-1}(L^{-1} - (1 - \beta)\Psi)^{-1} I_{\mathrm{S}}. \tag{25}$$

This matrix is full, and can be quite substantial if the front is complex. We use the symmetric solver in LinPack; approximations to this equation and faster summation techniques will be discussed in later work.

3.4.2. *Iterative solution of integral equation.* We now consider a different approach, which is to construct an iterative solution to the integral equation, which consists of a series expansion in the interaction matrix. Suitably interpreted, this can be viewed as a "multibounce" model, in which the number of terms in the series expansion corresponds to the number of bounces that a particle can undergo before its effects are negligible. This approach will allow us to check the error remainder term in this iterative formulation to determine how many terms must be kept. Since most of the particles either stick or leave the domain after a reasonable number of bounces, this is an effective approach.

We begin by defining the reflected intensity $I_{\mathrm{R},k}$ after the kth bounce, namely

$$I^i_{\mathrm{R},1} = (1 - \beta_0) I^i_{\mathrm{S}}, \tag{26}$$

$$I^i_{\mathrm{R},k+1} = (1 - \beta) \sum_{j, j \neq i} I^j_{\mathrm{R},k} \frac{\cos(\theta^j_i)\cos(\theta^i_j)}{2r_{ij}} \Upsilon_{ij} l_j. \tag{27}$$

In a matrix form, this becomes

$$I_{\mathrm{R},0} = (1 - \beta_0) I_{\mathrm{S}}, \tag{28}$$

$$I_{\mathrm{R},k+1} = (1 - \beta)\Omega I_{\mathrm{R},k}, \tag{29}$$

where Ω is defined as before. Now, define $I_{\mathrm{S},k}$ to be the position that sticks at the kth bounce. We then have that

$$I_{\mathrm{S},0} = \beta_0 I_{\mathrm{S}}, \tag{30}$$

$$I_{\mathrm{S},1} = \beta\Omega(1 - \beta_0) I_{\mathrm{S}}, \tag{31}$$

and, in general,

$$I_{\mathrm{S},k+1} = \frac{\beta}{1 - \beta} I_{\mathrm{R},k+1} = (1 - \beta)\Omega I_{\mathrm{S},k}. \tag{32}$$

Therefore, by reaching back to the initial expression, we have

$$I_{\mathrm{S},k} = \beta(1 - \beta)^{k-1}(1 - \beta_0)\Omega^k I_{\mathrm{S}}, \tag{33}$$

and thus the total intensity after N applications is given by

$$I_N = \beta(1 - \beta_0) \left[\sum_{k=1}^{N} (1 - \beta)^{k-1} \Omega^k \right] I_{\mathrm{S}} + \beta_0 I_{\mathrm{S}}. \tag{34}$$

Each application of the operator may be viewed as either an additional term in the expansion or an additional included bounce.

We note that there is a recurrence relation for I_N given by

$$\begin{aligned}
I_{N+1} &= \beta(1-\beta_0)\left[\sum_{k=1}^{N+1}(1-\beta)^{k-1}\Omega^k\right]I_S + \beta_0 I_S \\
&= \beta(1-\beta_0)\left[(1-\beta)\Omega\sum_{k=1}^{N}(1-\beta)^{k-1}\Omega^k + \Omega\right]I_S + \beta_0 I_S \\
&= (1-\beta)\Omega(I_N - \beta_0 I_S) + \beta(1-\beta_0)\Omega I_S + \beta_0 I_S \\
&= (1-\beta)\Omega I_N + (\beta-\beta_0)\Omega I_S + \beta_0 I_S.
\end{aligned}$$

By constructing the remainder term $I_{N+1} - I_N$, we can measure the convergence of the expansion and keep enough terms to bound the error below a user-specified tolerance.

4. ADDITIONAL NUMERICAL ISSUES

4.1. *Constructing Extension Velocity Fields*

The above produces the solution to the speed function F at each of the control points x_i. In order to use a level set approximation, an "extension" velocity field (see [44]) must be constructed which provides a velocity field for the neighboring level sets based on F at the control points. One technique is to stand at each grid of the narrow band and simply use the value from the closest point on the front; see [4, 5]. Given a narrow band of radius k, we can find the closest point in $O(k^2)$ in 2D and $O(k^3)$ in 3D. Thus, the total cost for the tube is $O(Nk^3)$ for 2D and $O(N^2k^4)$ in 3D. Another drawback of this method is that away from the front the speed will be discontinuous, which will result in corners and kinks in nonzero level sets.

Here, we introduce a different extension technique based on Sethian's Fast Marching Method for solving the eikonal equation, which was introduced in [42, 43]. The technique allows one to build an extension velocity field for the general situation in which a velocity must be extended from the front to points within a narrow band and may be used in a wide collection of applications. The cost will be $O(Nk\log(N))$ in two dimensions and $O(N^2k\log(N))$ in three dimensions. As an added benefit, it produces a smooth function off the front. There will still be discontinuities at those grid points where two or more points on the front are the same distance away; however, the stair-stepping exhibited by the previously described pure extension method is not present.

Briefly, the Fast Marching Method is a technique for solving the eikonal equation

$$|\nabla\phi|F = 1. \tag{35}$$

The technique relies on a combination of narrow band methods, upwind schemes, and a fast sorting algorithm. To imagine an easy case, consider a speed function

$F = 1$; thus in this case the goal is to compute the distance function from the initial front. The Fast Marching Method works by propagating the distance values away from the front. At any time the points being considered are approximately the same distance away from the initial front (give or take a grid cell). When a new point is updated, the values from points with smaller values are used to get a new crossing time. By using a heap sort algorithm, the Fast Marching Method allows one to systematically construct these distance grid values by always marching in upwind fashion, and hence, there is never a need to revisit a point once it is updated. If there are N **total** computational points in the domain, the fast marching method computes the solution to the eikonal equation in the complete domain in $O(N \log N)$ steps. As such, it is one of the fastest possible techniques for computing the solution to the eikonal equation. For details, see [42–44].

To construct an extension velocity field we use a similar idea. The crossing times are found as if the front is advancing with constant speed 1, but rather than only associate distances with each point, we also associate distances and extended values with each point. When the crossing time gets updated at a point, its extended value also gets updated, using the extended values of the points that are used to update the crossing time. The simplest method is to use weighted averaging depending on the difference between the new crossing value and the crossing value at the neighboring points.

Algorithmically, we have

- For the points next to the initial front, specify distance and extension values by using the neighboring points. Extension values are constructed by weighting the nearby values with the distance. These points will be the initial tentative points, and points that lie exactly on the front will be the only accepted points.
- As in the standard Fast Marching Method, pick the smallest tentative crossing time. For each neighboring point that has not been accepted, calculate a new crossing time. This calculation will choose one or two points in two dimensions, and up to three points in three dimensions. Once that crossing time is found, the extension value is set to the weighted average of the extension values from the points used in the crossing time calculation. The weight is proportional to the difference between the newly found crossing value and the crossing value at that point. For complete details about the use of Fast Marching Methods to construct extension velocities; see [3].

5. RESULTS

5.1. *Basic Calculations*

We begin with a straightforward calculation of isotropic etching into a hole, taken from [5]. In Fig. 3 we show a square hole from which a material is being isotropically etched; this corresponds to a simple speed function of $F = -1$. As expected, the sides of the cavity are cleanly etched away, leaving smoothed, rounded walls.

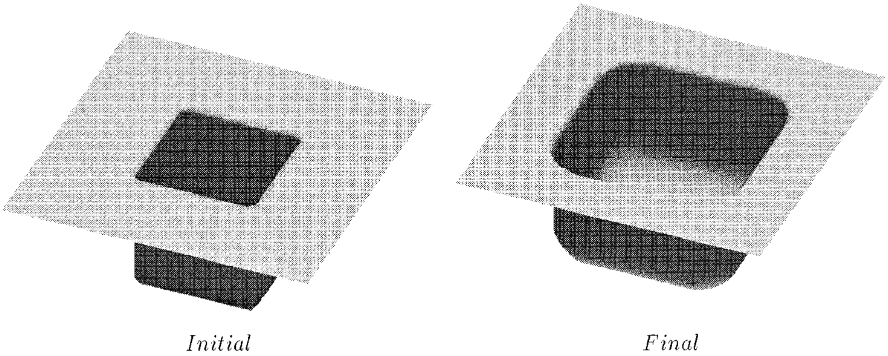

FIG. 3. Isotropic etching into a hole.

We follow with a calculation of source deposition from a plate located above the hole. The effects of visibility and shading are included. Along the entire plate, deposition material is emitted uniformly in each direction. In Fig. 4, we show two three-dimensional time plots of the evolving profile. The trench begins to pinch off due to the effects of visibility, and a bulb-shaped profile evolves.

We end the basic calculations section with the modeling (Fig. 5) of the effect of a nonconvex sputter etch/ion milling of a saddle surface. The nonconvex speed law $F = (1 + 4\sin^2(\theta))\cos(\theta)$ causes faceting of sharp corners and rounded polishing; for details of this effect, see [5].

5.2. *Test Cases: Reemission/Redeposition Simulations*

We begin with straightforward studies of etching and redeposition. In Fig. 6, etching occurs under the influence of a unidirectional etching beam coming straight down from the vertical. In Fig. 6a, there is no redeposition; however, in Fig. 6b, an amount of material equal to the amount etched is reemitted as a point source at the etching point and redeposited elsewhere on the front; that is, constant volume is maintained between the etching process and the reemission process.

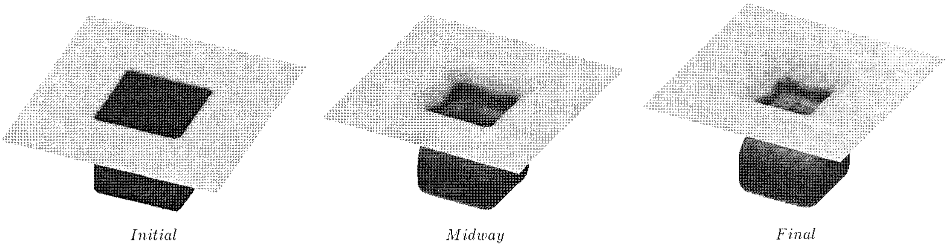

FIG. 4. Source deposition into a hole.

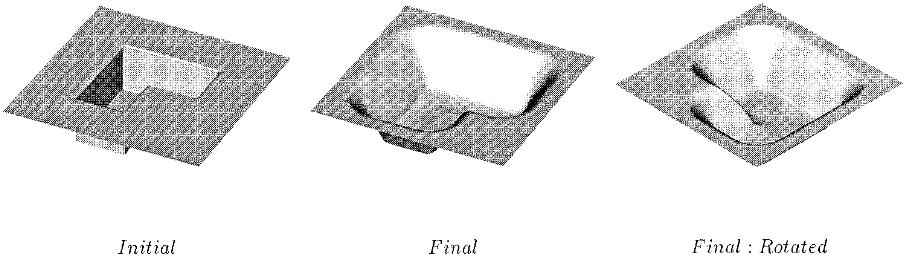

FIG. 5. Downward saddle under ion milling: $F = (1 + 4\sin^2(\theta))\cos\theta$.

Next, we consider a pure deposition process, in which the sticking coefficient is varied. In Fig. 7a, a unidirectional deposition beam enters from the vertical, and all of the material sticks (sticking coefficient 1.0). In Fig. 7b, the sticking is $\beta = 0.5$. In Fig. 7c, the sticking coefficient is $\beta = 0.2$. For sticking coefficient values less than unity, the matrix equation is solved. As the sticking coefficient decreases, the deposition layer becomes more uniformly distributed.

5.3. *Complex Examples*

We now follow with a collection of more complex simulations designed to demonstrate various physical effects.

5.3.1. *Parameter study.* We begin with a two-dimensional parameter study of the simultaneous effects of etching and deposition, without the effects of redeposition and reemission. We use a speed function,[3]

$$F = (1 - \alpha)F_{\text{etch}} + \alpha F_{\text{Deposition}}, \tag{36}$$

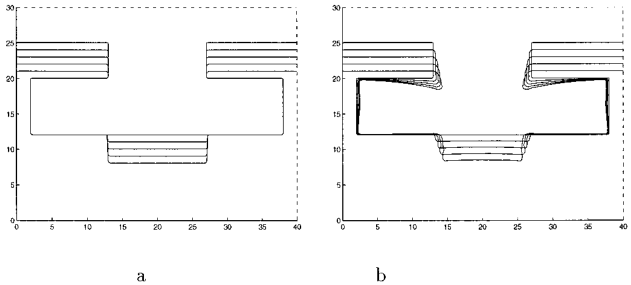

FIG. 6. Effect of redeposition on unidirectional etching process: (a) etching; (b) etching plus redeposition.

---

[3] This form for the ion-milling term was suggested by J. Rey of Technology Modeling Associates.

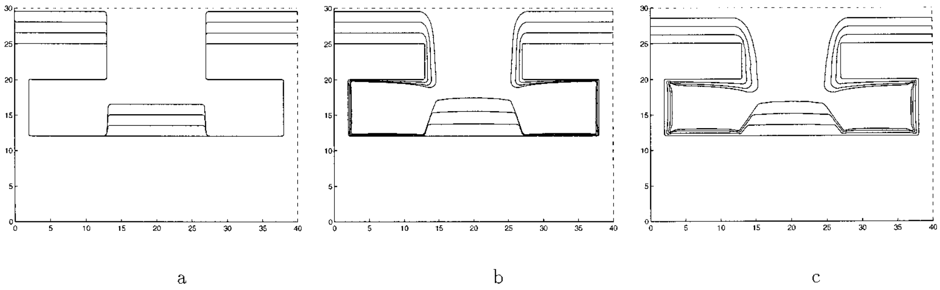

FIG. 7. Effect of varying sticking coefficient on deposition/redeposition: (a) sticking coefficient 1.0; (b) sticking coefficient 0.5; (c) sticking coefficient 0.2.

where

$$F_{\text{etch}} = (5.2249 \cos \theta - 5.5914 \cos^2 \theta + 1.3665 \cos^4 \theta), \tag{37}$$

$$F_{\text{Deposition}} = \beta F_{\text{Isotropic}} + (1 - \beta) F_{\text{Source}}. \tag{38}$$

As shown in [4, 5], ion-milling terms of this form yield nonconvex Hamiltonian–Jacobi equations and must be computed using appropriate upwind schemes. Visibility effects are considered in all terms except isotropic deposition. The results of varying α and β between 0 and 1 are shown in Fig. 8.

5.3.2. *Trench depth on reemission profiles.* Next, we study the relationship between body geometry and reemission profiles. In Fig. 9, we show a 3×3 matrix displaying the interplay between body geometry and various for the sticking coefficient. We assume a unidirectional deposition beam, and a sticking coefficient of β means that $1 - \beta$ of the material is not deposited but instead reemitted as a point source.

We repeat the study in Fig. 10, only this time we assume deposition from a line source above the trench. In both cases, as the depth of the cavity decreases, more reemission comes from the bottom of the cavity, and the deposition spread is more uniform. Furthermore, in both cases we observe a slight lagging of the front in corners; this is due to leakage in our discretization of the integral for the front. This problem can be corrected with a nonuniform discretization scheme, which is discussed elsewhere; see [29]:

$$F = (1 - \alpha) F_{\text{etch}} + \alpha F$$

$$F_{\text{etch}} = (5.2249 \cos \theta - 5.5914 \cos^2 \theta + 1.3665 \cos^4 \theta) \cos \theta$$

$$F_{\text{Deposition}} = \beta F_{\text{Isotropic}} + (1 - \beta) F_{\text{Source}}.$$

5.3.3. *Multiple effects.* An important simulation is obtained by considering a periodic sequence of structures under the multiple effects of ion-milling, isotropic deposition, and redeposition. Here, the goal is to model the faceting that occurs due to the nonconvexity of the ion-milling term (see [4, 5]), as well as the role of

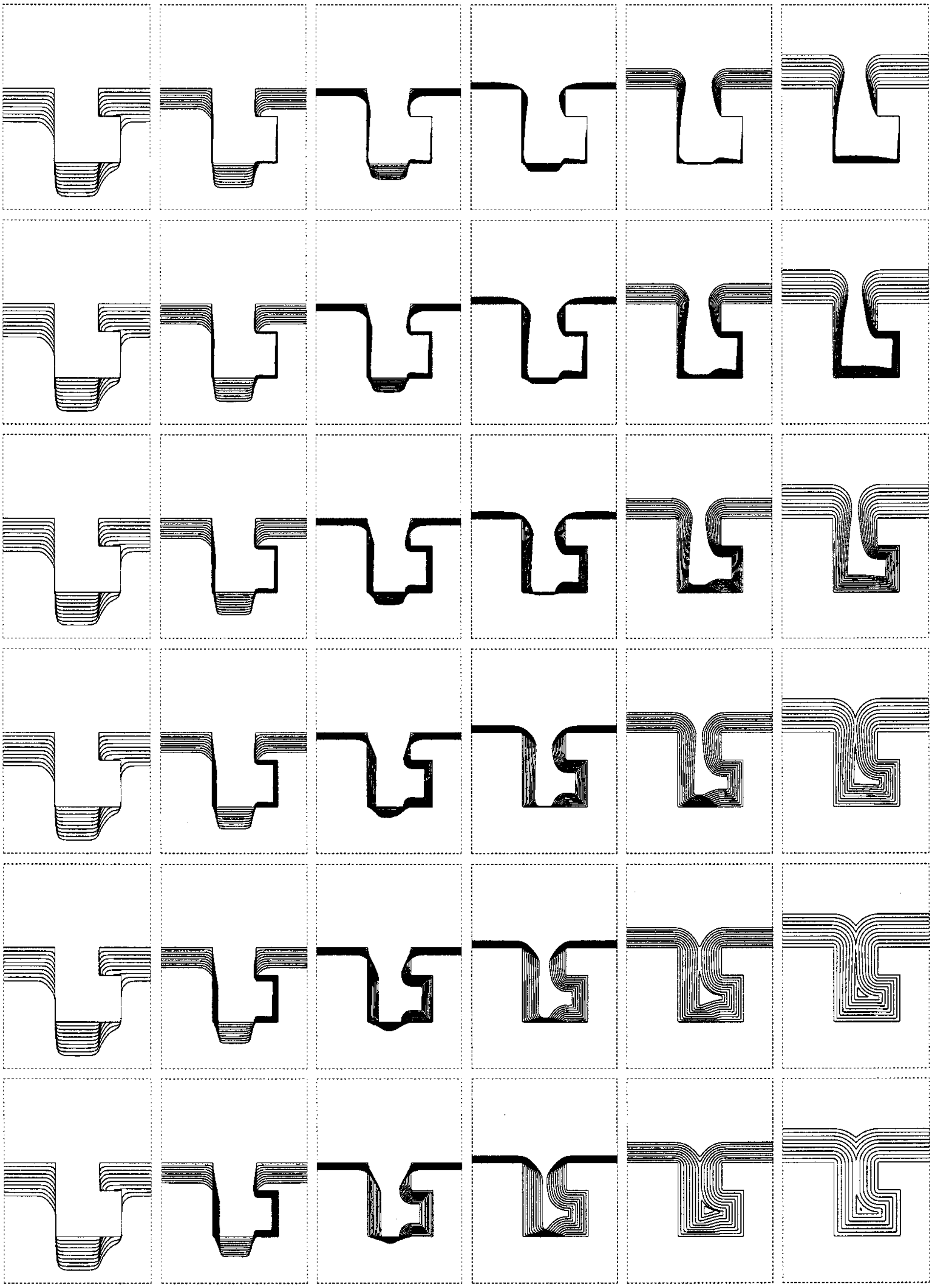

FIG. 8. Simultaneous etching and deposition: α increases from left to right; β increases from top to bottom.

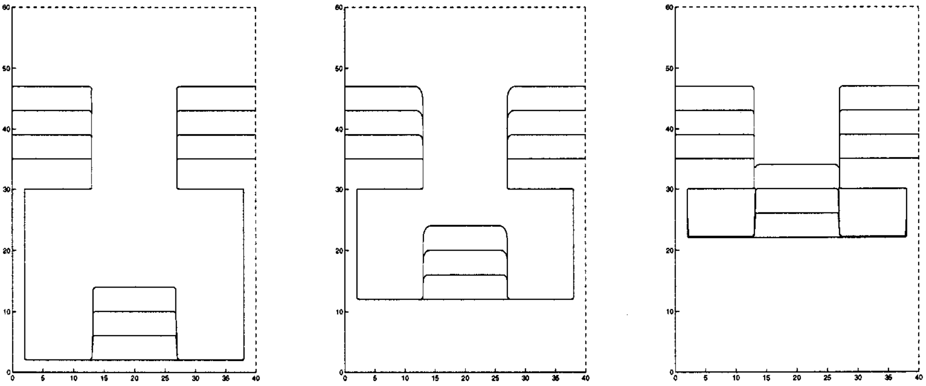

Sticking Coefficient=1.0

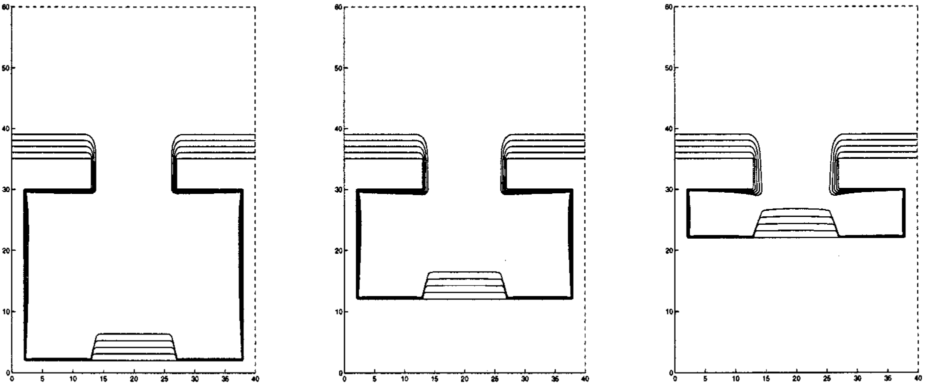

Sticking Coefficient=.5

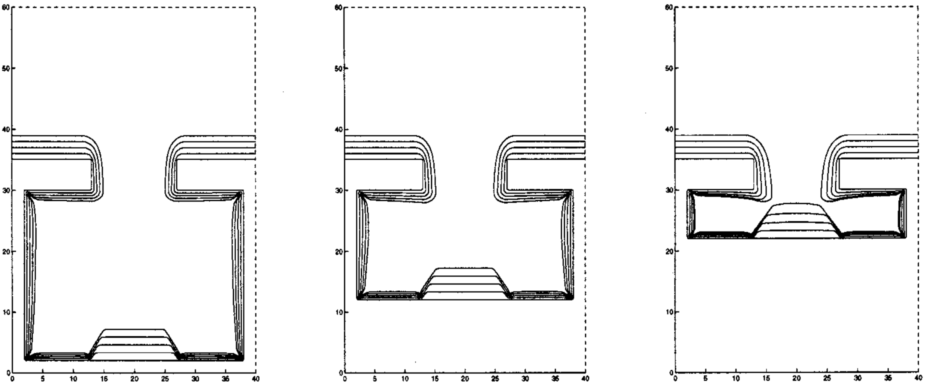

Sticking Coefficient=.2

FIG. 9. Body geometry versus sticking coefficient: unidirectional deposition.

redeposition in rounding sharp corners as a function of the reemission coefficient. A combination of ion-milling and ion-induced sputtered redeposition is shown in Fig. 11, together with conformal deposition and direct deposition. On the left, the ion-induced sputter redeposition is set to zero; on the right the etched material is reemitted, producing considerable rounding of the sharp corners.

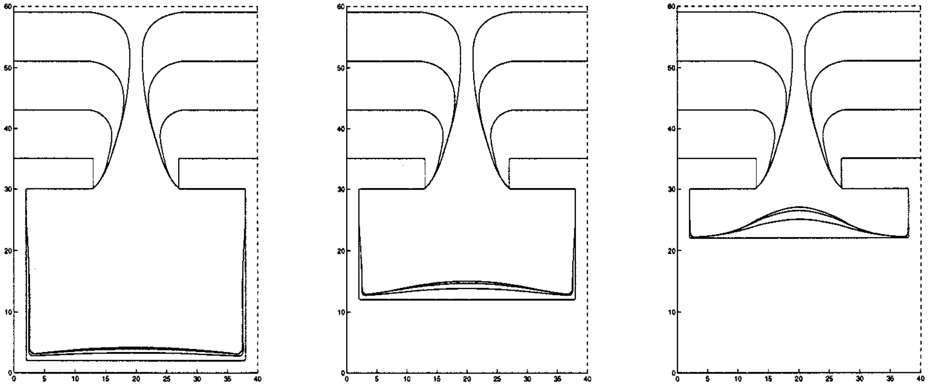

Sticking Coefficient=1.0

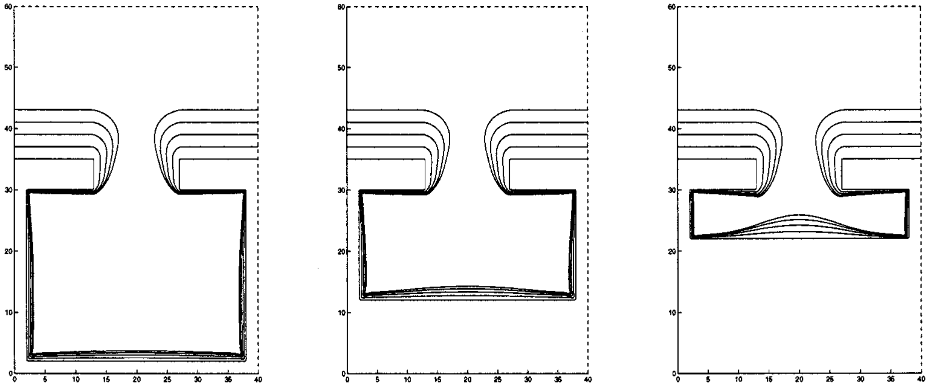

Sticking Coefficient=.5

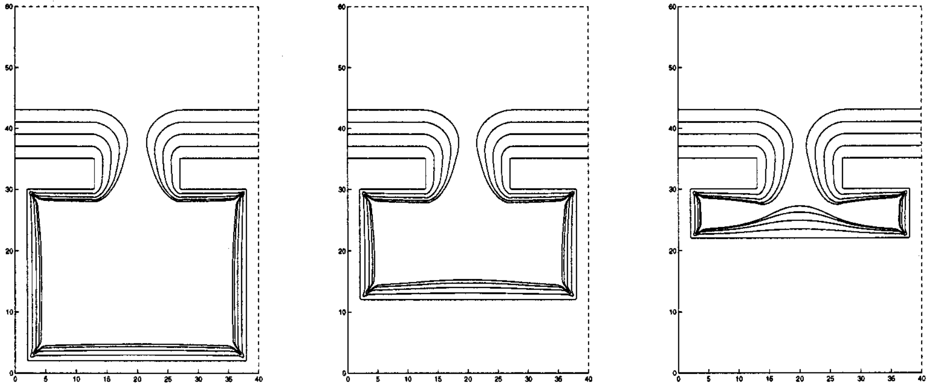

Sticking Coefficient=.2

FIG. 10. Body geometry versus sticking coefficient: line source deposition.

Next, we consider a complex speed function,[4] which consists of a sensitive angle-dependent speed law. A plot of the speed as a function of θ shows that for some values of θ, deposition dominates over etching, while for other values, etching is

---

[4] This example was suggested by J. Rey of Technology Modeling Associates.

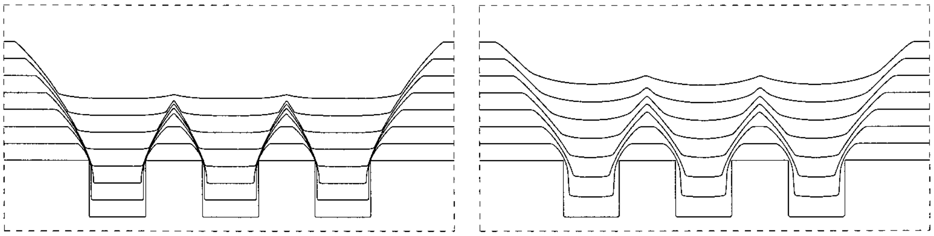
No re-deposition

With re-deposition

FIG. 11. Combination of ion-milling, direct deposition, and conformal deposition.

the dominant effect. We further add the restriction that the initial structure is impenetrable and thus cannot be etched. In Fig. 12, we show the effect of the speed law

$$F = (4.385 - 5.7 \cos \theta + 1.425 \cos^3 \theta)\cos \theta \tag{39}$$

on a periodic structure. We observe that the impenetrability of the material forces the selection of two critical angles, as seen in the sharp angles at the protruding corners of the structure.

5.3.4. *Thin films and nanolayers.* Next, we consider a problem in which several effects are combined. We imagine an initial block, in which a mask covers a substrate, and we envision a simultaneous etch and deposition process. We imagine that one material (which will be shown as light gray) is isotropically deposited on both the mask (shown in dark gray) and substrate (shown in black). At the same time that this material is being deposited, it is being etched under an ion-milling/sputter law, such that the etch rate in the substrate is twice as fast as the etch rate in the mask. Thus, we have

$$F = F_{\text{IsotropicDeposition}} + F_{\text{SputterEtching}} \tag{40}$$

$$F_{\text{IsotropicDeposition}} = 0.5; F_{\text{SputterEtching}} = \text{Factor}(x) * \cos \theta: \tag{41}$$

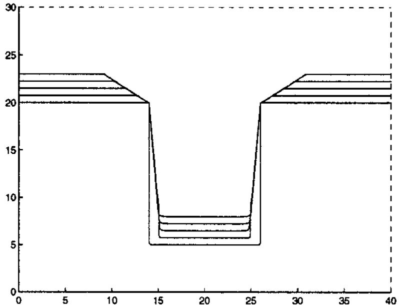

FIG. 12. Impenetrable block under simultaneous etching and deposition.

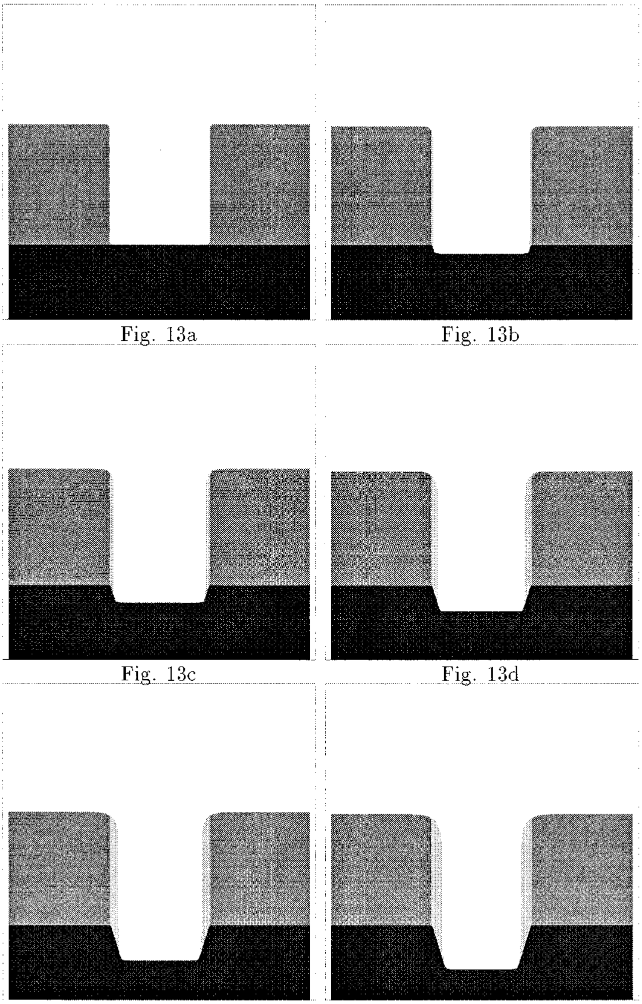

Fig. 13a Fig. 13b

Fig. 13c Fig. 13d

Fig. 13e Fig. 13f

FIG. 13. Combination of isotropic deposition of thin layer and convex sputter etching of materials, time sequence:

$$F = F_{\text{IsotropicDeposition}} + F_{\text{SputterEtching}} \tag{42}$$

$$F_{\text{IsotropicDeposition}} = 0.5, \quad F_{\text{SputterEtching}} = \text{Factor}(x) * \cos\theta \tag{43}$$

Factor(x) $= 1.0$ if in mask (dark gray)/Factor(x) $= 2.0$ if in substrate (black).

- Factor(x) $= 1.0$ if in dark gray material (mask),
- Factor(x) $= 2.0$ if in black material (substrate).

In Fig. 13, we show the sequence of profile evolution under these effects. We note the development of the thin nano-layer which covers the side walls, but is fully etched away along the top and the bottom; we also note the existence of evolving points where several fronts touch. We stress that the grid used for this calculation is *significantly larger* than the size of the nano-layer; thus our algorithms provide for significant subgrid resolution without resorting to adaptive mesh technology; see [44] for details of this technology.

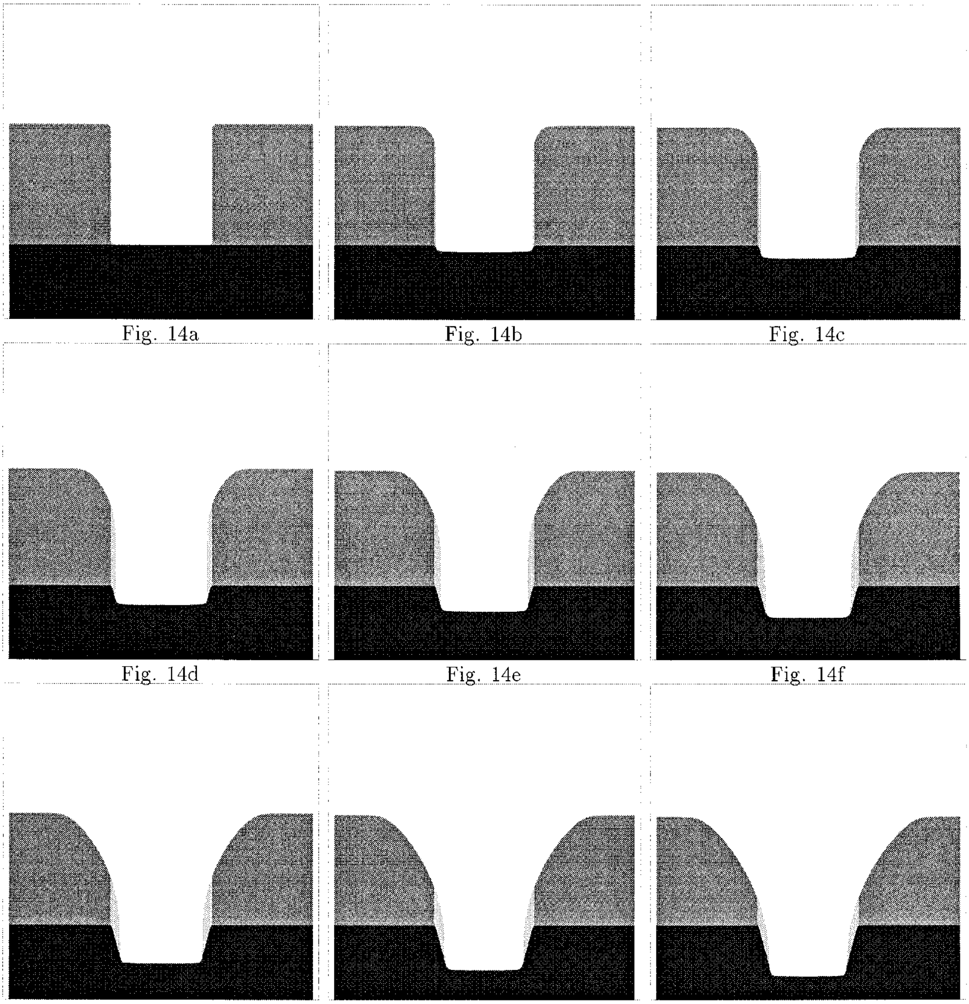

Fig. 14a Fig. 14b Fig. 14c

Fig. 14d Fig. 14e Fig. 14f

Fig. 14g Fig. 14h Fig. 14i

FIG. 14. Combination of isotropic deposition of thin layer and nonconvex sputter etching of materials, time sequence:

$$F = F_{\mathrm{IsotropicDeposition}} + F_{\mathrm{SputterEtching}} \tag{44}$$

$$F_{\mathrm{IsotropicDeposition}} = 0.5, \quad F_{\mathrm{SputterEtching}} = \mathrm{Factor}(x) * (1. + 4\sin^2\theta)\cos\theta \tag{45}$$

$\mathrm{Factor}(x) = 1.0$ if in mask (dark gray)/$\mathrm{Factor}(x) = 2.0$ if in substrate (black).

We repeat the calculation in Fig. 14, only this time using an ion-milling sputter etching speed law which promotes faceting due to the presence of nonconvex Hamiltonians; see [4, 5]. Here, we note the rounding of the side wall layers, as well as the existence of multiple fronts and thin layer structures.

5.3.5. *Surface diffusion.* Two types of surface diffusion can play important roles in coverage and deposition layers; bulk diffusion, which is the global macro-motion of the material within the deposited layer, and surface diffusion, which relates to the motion of metal boundaries. Here, we examine the effects of surface diffusion on the shape of the deposition layer.[5]

Cale and Jain [7, 23] have performed carefully fit numerical experiments to match experimental evidence of surface diffusion effects of aluminum-(1.5%) copper films. They propose (see Cale and Jain [7], and Cale and Raupp [8–10]) a model of the form

$$\eta(s) - R(s) + \text{const}\,\frac{\partial^2 \kappa}{\partial s^2} = 0, \tag{46}$$

where $\eta(s)$ is the ballistic flux of atoms arriving at the surface position s, $R(s)$ is the rate of incorporation of atoms into the solid film, and κ is the signed curvature. We refer the reader to [8–10] for a detailed discussion of transport equations and related terms.

Here, we analyze a model problem which contains the effects of surface motion driven by surface diffusion. We recall the level set formulation

$$\phi_t + F|\nabla\phi| = 0. \tag{47}$$

A wide collection of problems have been studied when the speed function F is of the form

$$F = 1 - \varepsilon\kappa, \tag{48}$$

where κ is the curvature of the interface (see [44]). In the case of surface diffusion, we need to solve a model problem of the form

$$F = 1 + \varepsilon\kappa_{\alpha\alpha}, \tag{49}$$

where α is an arc-length parameterization. This is suggestive of the well-known sintering equations, which have been analyzed using a level set formulation by Chopp and Sethian in [15]; see also [44]. Briefly, while flow under curvature $F = \kappa$ causes all closed simple curves to become circular, shrink to a point and disappear [21], any circle is stable under motion by the second derivative of curvature $F = \kappa_{\alpha\alpha}$. We know of no formal proofs for limiting states of such curves analogous to the one Grayson proved for motion under curvature [21]. Numerical evidence so far indicates that convex curves become circular and then stop; detailed numerical studies may be found in [15].

The problem is delicate because Eq. (49) is a time-dependent fourth-order partial differential equation, and the presence of the fourth derivative requires an exceedingly small time step for stability in an explicit scheme; the linear fourth-order heat equation has a stability time step requirement of the form $O(\Delta t/\Delta h^4)$. Such schemes can in fact be made implicit to allow a larger time step; see [15] for further discussion.

It is tempting to alter the equation and create a surface diffusion model by using a speed function of the form $F(\kappa) = -\varepsilon\kappa$, since, for a short time this probably gives

---

[5] We thank T. Cale and J. Rey for illuminating conversations about the role and effects of surface diffusion.

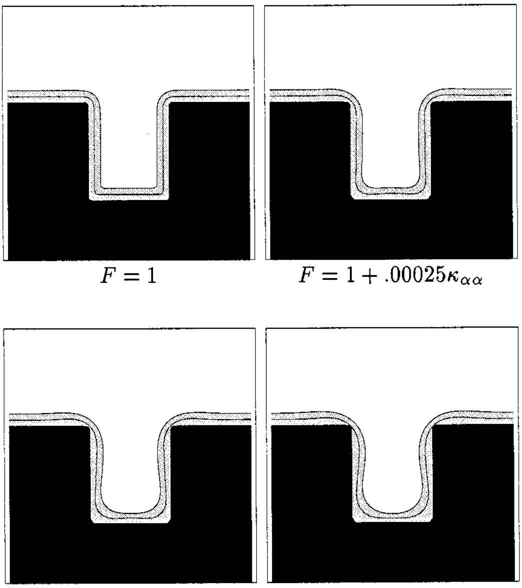

$F = 1$ $\quad$ $F = 1 + .00025\kappa_{\alpha\alpha}$

$F = 1 + .001\kappa_{\alpha\alpha}$ $\quad$ $F = 1 + .002\kappa_{\alpha\alpha}$

FIG. 15. Effects of surface diffusion on isotropic deposition: $F = 1 - \varepsilon\kappa_{\alpha\alpha}$.

effects close to the actual sintering equation, and the time step requirement is considerably less drastic. Nonetheless, we have chosen to work with the full fourth-order equation.

We can convert the problem to a level set formulation by differentiating the curvature expression twice in the tangent direction along each level line. Following the discussion in [15], we have

$$\phi_t + (1 + \varepsilon\kappa_{\alpha\alpha})|\nabla\phi| = 0 \tag{50}$$

$$\phi_t + |\nabla\phi| = -\varepsilon\left[\nabla\cdot\frac{\nabla\phi}{|\nabla\phi|}\right]_{\alpha\alpha} \tag{51}$$

$$\phi_t + |\nabla\phi| = -\varepsilon\nabla\left[\nabla\left[\nabla\cdot\frac{\nabla\phi}{|\nabla\phi|}\right]\cdot\frac{\phi_y, -\phi_x}{|\nabla\phi|}\right]\cdot\frac{\phi_y, -\phi_x}{|\nabla\phi|}. \tag{52}$$

We use a central difference approximation for the derivatives, and regularize the denominator to avoid the singularity associated with vanishing gradients.

We begin in Fig. 15 by showing the effects of surface diffusion on a model problem of isotropic deposition; that is, we examine a speed function $F = 1 + \varepsilon\kappa_{\alpha\alpha}$ for varying values of ε.

We next turn to a more realistic case and consider a speed function which contains isotropic deposition and an ion-milling nonconvex etch function, together with surface diffusion; that is, in Fig. 16 we consider the speed function

$$F = 4 - (1 + 4\sin^2\theta)\cos(\theta) + \varepsilon\kappa_{\alpha\alpha} \tag{53}$$

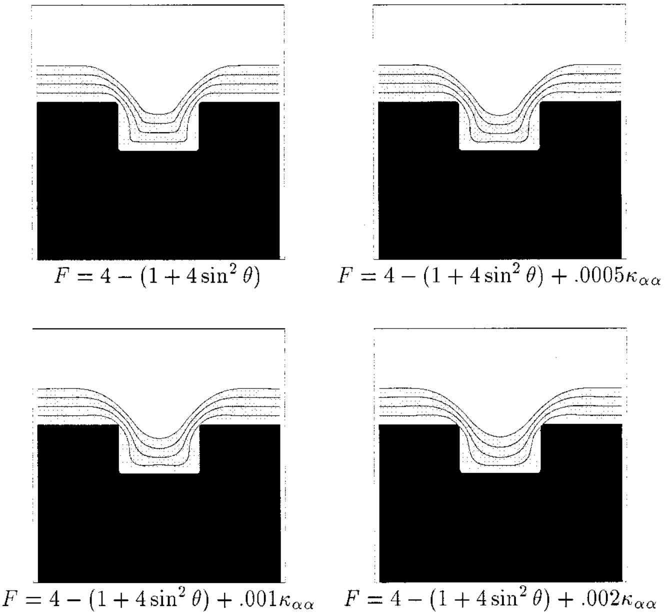
$F = 4 - (1 + 4\sin^2\theta)$

$F = 4 - (1 + 4\sin^2\theta) + .0005\kappa_{\alpha\alpha}$

$F = 4 - (1 + 4\sin^2\theta) + .001\kappa_{\alpha\alpha}$

$F = 4 - (1 + 4\sin^2\theta) + .002\kappa_{\alpha\alpha}$

FIG. 16. Effects of surface diffusion on deposition plus ion-milling: $F = 4 - (1 + 4\sin^2\theta) + \varepsilon\kappa_{\alpha\alpha}$.

5.4. *Three-Dimensional Effects*

Finally, we end with three examples showing three-dimensional problems which include the effects of a low sticking coefficient on deposition/redeposition. In Fig. 17, we show the effects of a small sticking coefficient on a three-dimensional struc-

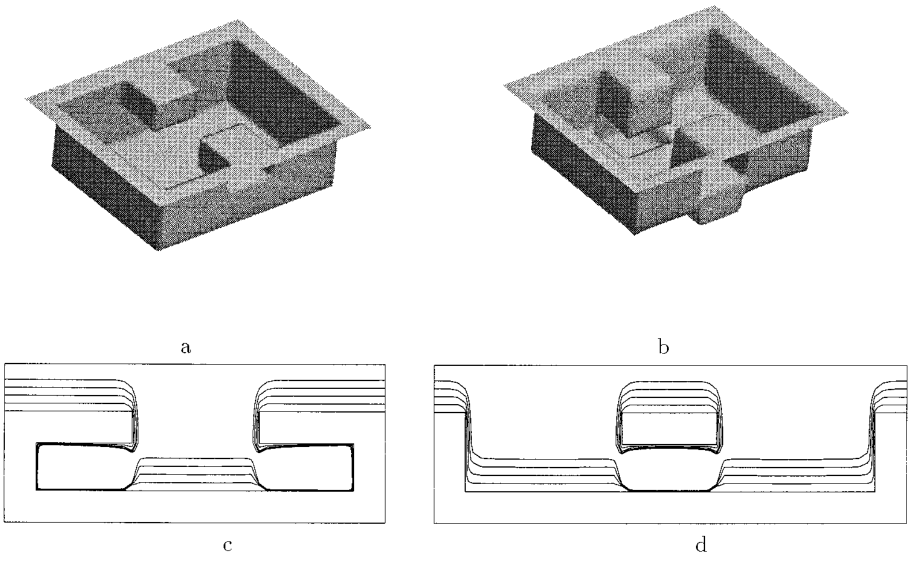

FIG. 17. Effects of low sticking coefficient (0.1) on 3D structure: (a, c) initial 2D cross section through both pegs; (b, d) later, 2D cross section (noncentered) through single peg.

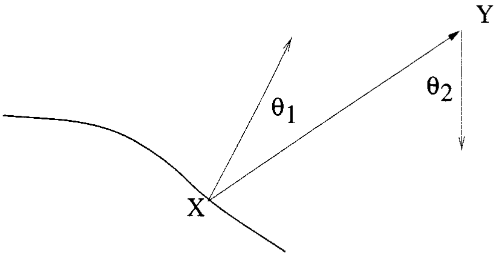

FIG. 18. Variables for double-L simulations.

ture. While the structure is somewhat unrealistic, it is chosen to illustrate the effects under study. The structure is a rectangular trench, with pegs protruding in from opposite sides. In Fig. 17a, we show the initial three-dimensional shape, followed in Fig. 17b by a later configuration. Here, the effect of the deposition is to create a layer everywhere except under the pegs, while the effects of the redeposition is to create a layer *underneath* the overhang. Next, in Fig. 17c and Fig. 17d, we show two-dimensional cross sections of the evolving profile, which better illustrate the effects of the redeposition.

Finally, we perform two studies of complex motions applied to a double-L shape. We begin with a study which balances source distribution with an angular flux cosine dependence with an isotropic deposition term. That is, let the Flux(x) received at a point x on the surface emitted from a point y on the source be given by

$$\text{Flux}(x) = 0.9\cos(\theta_1)\cos(\theta_2) + 0.1, \tag{54}$$

where θ_1 is the angle that the vector v from x to y makes with the normal at x, and θ_2 is the angle that the vector v makes with the vertical. Figure 18 shows the variables for this expression. This flux is integrated over the entire source to obtain the speed function F at the point x.

In Fig. 19, we show the double-L shape under the effects of this flux distribution.

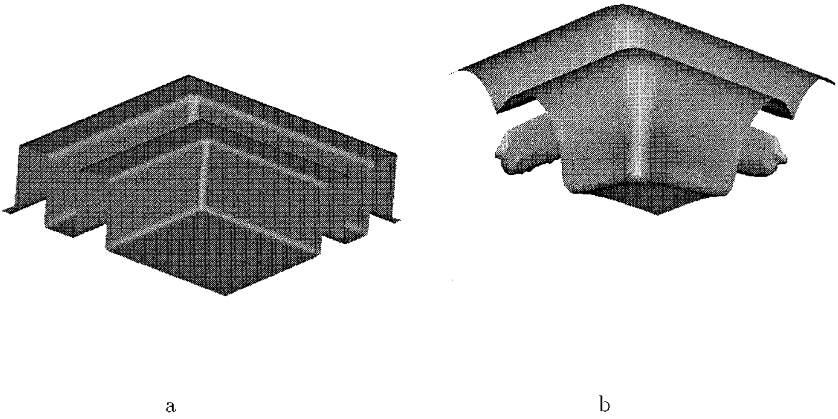

FIG. 19. Three-dimensional evolution under cosine source distribution and isotropic deposition: (a) initial shape; (b) later.

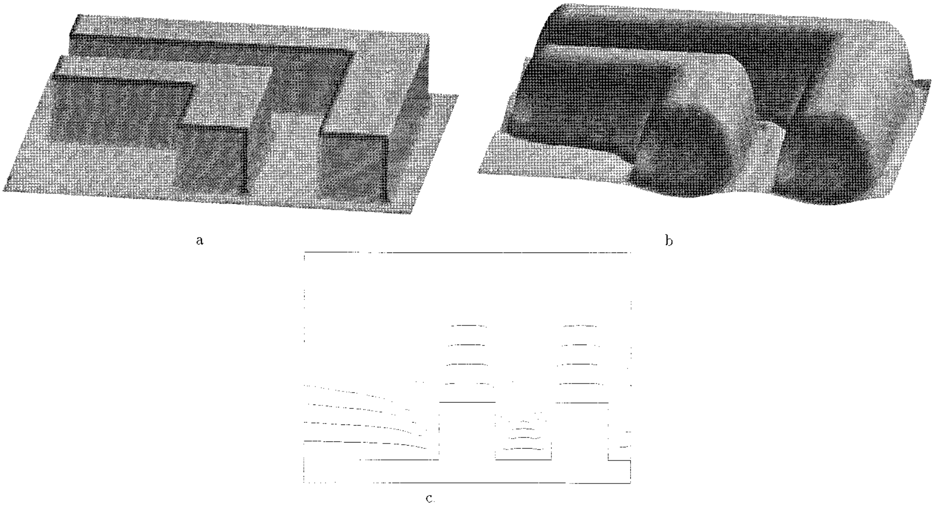

FIG. 20. Three-dimensional evolution under cosine source distribution with sticking coefficient 0.1: (a) initial position; (b) time evolution; (c, d) cross section.

Figure 19a, we show the initial shape from a diagonal angle; the development of a void is clearly shown in the three-dimensional profile shown in Fig. 19b.

Finally, in Fig. 20, we repeat the calculation using the initial shape shown in Fig. 20a. However, this time we remove the isotropic deposition term and consider a combination of two cosine flux deposition sources. That is, the initial flux at each point is given by

$$\mathrm{Flux}(x) = \cos^5(\theta_1)\cos(\theta_2) + \cos(\theta_1)\cos(\theta_2); \tag{55}$$

in addition, the second deposition term is given a sticking coefficient of 0.1, thus we also consider the effects of redeposition. We see that in this case, the void does not form; results are shown after some time evolution in Fig. 20b; a two-dimensional cross-sectional cut is shown in Fig. 20c.

6. TIMINGS

The computational labor required in these calculations is most directly a function of the grid resolution required to represent the front and the complexity of the physical effects under consideration. In Table I and II rough timings are given for various sizes and physical complexities for a Sun Ultra. The lithography timings were computed using the fast marching method given in [43].

This paper formulates a level set approach to handle a wide collection of complex topographic problems in etching and deposition. The next step, currently underway, is to couple this methodology to Navier–Stokes solvers for computing the relevant fluid effects off the front and to provide hydrodynamic and transport links between

TABLE I
Two-Dimensional Timings

Test	50 by 50 Runtime	 Steps	 Time/step	100 by 100 Runtime	 Steps	 Time/step
Lithography (fast marching)	6.9 ms	NA	NA	26 ms	NA	NA
Isotropic (narrow band)	82 ms	24	3.4 ms	0.4 s	49	8 ms
Unidirectional (with visibility)	0.4 s	17	23 ms	2.3 s	34	70 ms
Etching and redeposition	1.7 s	25	68 ms	14 s	51	0.3 s
Deposition and redeposition (iterative model)	1.1 s	17	65 ms	12 s	39	0.3 s

the surface evolution and physics in the interior; we shall report on this work elsewhere.

ACKNOWLEDGMENTS

All calculations were performed at the University of California at Berkeley and the Lawrence Berkeley National Laboratory. A video tape of the above simulations is available by request. We would like to thank L. Borucki, T. Cale, B. Coughran, J. Lee, P. Leon, A. Neureuther, C. Rafferty, J. Rey, V. Singh, K. Smith, and K. Toh for helpful discussions. A web page describing level set methods and this work in particular may be found at http://math.berkeley.edu/~sethian/level_set.html.

TABLE II
Three-Dimensional Timings

Test	40 by 40 by 40 Runtime	 Steps	 Time/step	80 by 80 by 80 Runtime	 Steps	 Time/step
Lithography (fast marching)	0.16 s	NA	NA	2.1 s	NA	NA
Isotropic (narrow band)	1.3 s	8	0.16 s	13.6 s	24	0.6 s
Unidirectional (with visibility)	16.7 s	24	0.7 s	270 s	47	5.7 s
Etching and redeposition	224 s	12	19 s	260 m	25	10 m
Deposition and redeposition (iterative model)	265 s	11	24 s	290 m	23	12.6 m

REFERENCES

1. D. Adalsteinsson, R. Kimmel, R. Malladi, and J. A. Sethian, *Fast Marching Methods for Computing Solutions to Static Hamilton–Jacobi Equations,* Center for Pure and Applied Mathematics Report, University of California at Berkeley, 1996. [SIAM J. Num. Anal, submitted]
2. D. Adalsteinsson and J. A. Sethian, A fast level set method for propagating interfaces, *J. Comput. Phys.* **118,** 269 (1995).
3. D. Adalsteinsson and J. A. Sethian, Fast Marching Methods for reinitialization and extension velocities in level set methods, to be submitted for publication.
4. D. Adalsteinsson and J. A. Sethian, A level set approach to a unified model for etching, deposition, and lithography I: Two-dimensional simulations, *J. Comput. Phys.* **120**(1), 128 (1995).
5. D. Adalsteinsson and J. A. Sethian, A level set approach to a unified model for etching, deposition, and lithography II: Three-dimensional simulations, *J. Comput. Phys.* **122**(2), 348 (1995).
6. S. Altshuler, S. B. Angenent, and Y. Giga, Mean curvature flow through singularities for surfaces of rotation, preprint, 1993.
7. T. S. Cale, M. K. Jain, C. J. Tracy, and R. Duffin, *J. Vac. Sci. Technol. B,* submitted.
8. T. S. Cale and G. B. Raupp, Free molecular transport and deposition in cylindrical features, *J. Vac. Sci. Technol. B* **8**(4), 649 (1990).
9. T. S. Cale and G. B. Raupp, Free molecular transport and deposition in long rectangular trenches, *J. Appl. Phys.* **68**(7), 3645 (1990).
10. T. S. Cale and G. B. Raupp, A unified line-of-sight model of deposition in rectangular trenches, *J. Vac. Sci. Tech., B,* **8**(6), 1242 (1990).
11. Y. C. Chang, T. Y. Hou, B. Merriman, and S. J. Osher, A level set formulation of eulerian interface capturing methods for incompressible fluid flows, *J. Comput. Phys.* **124**(2), 449 (1994).
12. Y. Chen, Y. Giga, and S. Goto, Uniqueness and existence of viscosity solutions of generalized mean curvature flow equations, *J. Diff. Geom.* **33,** 749 (1991).
13. D. L. Chopp, Computing minimal surfaces via level set curvature flow, *J. Comput. Phys.* **106,** 77 (1993).
14. D. L. Chopp and J. A. Sethian, Flow under curvature: singularity formation, minimal surfaces, and geodesics, *Jour. Exper. Math* **2**(4), 1994.
15. D. L. Chopp and J. A. Sethian, A level set approach to the numerical simulation of viscous sintering, work in progress, 1996.
16. L. C. Evans, H. M. Sonar, and P. E. Souganidis, Phase transitions and generalized motion by mean curvature, *Communications on Pure and Applied Mathematics* **45,** 1097 (1992).
17. L. C. Evans and J. Spruck, Motion of level sets by mean curvature, *J. Diff. Geom.* **33,** 635 (1991).
18. L. C. Evans and J. Spruck, Motion of level sets by mean curvature II, Transactions of the American Mathematical Society **330,** 91 (1992).
19. M. Falcone, T. Giorgi, and P. Loretti, Level sets of viscosity solutions and applications, Instituto per le Applicazioni del Calcolo, Rome, preprint, 1990.
20. Y. Giga and S. Goto, Motion of hypersurfaces and geometric equations, *Journal of the Mathematical Society of Japan* **44,** 99 (1992).
21. M. Grayson, The heat equation shrinks embedded plane curves to round points, *J. Diff. Geom.* **26,** 285 (1987).
22. G. Huisken, Flow by mean curvature of convex surfaces into spheres, *J. Diff. Geom.* **20,** 237 (1984).
23. M. K. Jain, T. S. Cale, C. J. Tracy, and R. L. Duffin, Curvature driven surface diffusion of aluminum–(1.5) copper during sputter deposition, in *Proceedings, 11th VMIC Conference, 1992.*
24. R. Kimmel and A. Bruckstein, *Shape from shading via level sets,* Center for Intelligent Systems Report No. 9209, Technion-Israel Institute of Technology, June 1992.
25. R. Malladi and J. A. Sethian, Image processing via level set curvature flow, *Proc. Natl. Acad. of Sci. USA* **92**(15), 7046 (1995).

26. R. Malladi and J. A. Sethian, Image processing: Flows under min/max curvature and mean curvature, *Graphical Methods in Image Processing,* **58**(2), 127 (1996).
27. R. Malladi, J. A. Sethian, and B. C. Vemuri, *Shape modeling with front propagation: A level set approach, IEEE Trans. Pattern Anal. Mach. Intell.* **17**(2), (1995).
28. J. P. McVittie, J. C. Rey, A. J. Bariya, and others, SPEEDIE: A profile simulator for etching deposition, *Proc. SPIE-The Int. Soc. Opt. Eng.* **1392,** 126 (1991).
29. B. Milne, Adaptive level set methods interfaces, Ph.D. thesis, Dept. of Mathematics, University of California, Berkeley, 1995.
30. W. Mulder, S. J. Osher, J. A. Sethian, Computing interface motion in compressible gas dynamics, *J. Comput. Phys.* **100,** 209 (1992).
31. S. Osher and J. A. Sethian, Fronts propagating with curvature dependent speed: Algorithms based on Hamilton–Jacobi formulation, *Jour. Comp. Phys.* **79,** 12 (1988).
32. S. Osher and C. Shu, High-order nonoscillatory schemes for Hamilton-Jacobi equations, *J. Comput. Phys.* **28,** 907 (1991).
33. J. C. Rey, Cheng, Lie-Yea, J. P. McVittie, K. C. Saraswat, Monte Carlo low pressure deposition profile simulations, *Journal of Vacuum Science and Technology A* (Vacuum, Surfaces, and Films), May–June 1991, **9**(3, pt. 1) 1083.
34. C. Rhee, L. Talbot, and J. A. Sethian, Dynamical study of a premixed V flame, *Jour. Fluid Mech.* **300,** 87 (1995).
35. E. W. Scheckler, Ph.D. dissertation, EECS, University of California, Berkeley, 1991.
36. E. W. Scheckler, K. K. H. Toh, D. M. Hoffstetter, and A. R. Neureuther, 3D lithography, etching and deposition simulation, in *Symposium on VLSI Technology, Oiso, Japan, 1991* p. 97.
37. J. A. Sethian, *An analysis of flame propagation,* Ph.D. dissertation, Mathematics, University of California, Berkeley, 1982.
38. J. A. Sethian, *Curvature and the evolution of fronts, Commun. Math. Physics.* **101,** 487 (1985).
39. J. A. Sethian, Curvature flow and entropy conditions applied to grid generation, *J. Comp. Phys.* **115,** 440 (1994).
40. J. A. Sethian, Numerical algorithms for propagating interfaces: Hamilton-Jacobi equations and conservation laws, *J. Diff. Geom.* **31,** 131 (1990).
41. J. A. Sethian, Numerical methods for propagating fronts, in *Variational Methods for Free Surface Interfaces,* edited by P. Concus and R. Finn (Springer-Verlag, New York, 1987).
42. J. A. Sethian, A review of the theory, algorithms, and applications of level set methods for propagating interfaces, *Acta Numer.* (1996).
43. J. A. Sethian, A fast marching level set method for monotonically advancing fronts, *Proc. Nat. Acad. Sci.,* **93,** 4 (1996).
44. J. A. Sethian, *Level set methods: evolving interfaces in geometry, fluid mechanics, computer vision and material science,* Cambridge University Press, 1996.
45. J. A. Sethian and D. Adalsteinsson, An overview of level set methods for etching, deposition, and lithography development, IEEE Transactions on Semiconductor Devices **10**(1), 167 (1997).
46. J. A. Sethian and J. D. Strain, Crystal growth and dendritic solidification, *J. Comput. Phys.* **98,** 231 (1992).
47. V. K. Singh, S. G. Shaqfeh, and J. P. McVittie, Simulation of profile evolution in silicon reactive ion etching with reemission and surface diffusion, *J. Vac. Sci. Tech., B.* **10**(3), 1091 (1993).
48. K. K. H. Toh, Ph.D. Dissertation, EECS, University of California, Berkeley, (1990).
49. K. K. H. Toh and A. R. Neureuther, Three-dimensional simulation of optical lithography, Proceedings SPIE, Optical/Laser Microlithography IV, **1463,** 356 (1991).
50. J. Zhu and J. A. Sethian, Projection methods coupled to level set interface techniques, *J. Comp. Phys.* **102,** 128 (1992).